

Deep generative modeling for probabilistic forecasting in power systems

Jonathan Dumas^{a,*}, Antoine Wehenkel^a, Damien Lanaspeze^b, Bertrand Cornélusse^a, Antonio Sutera^a

^aLiège University, Departments of Computer Science and Electrical Engineering, Belgium
^bMines ParisTech, France

Abstract

Greater direct electrification of end-use sectors with a higher share of renewables is one of the pillars to power a carbon-neutral society by 2050. This study uses a recent deep learning technique, the *normalizing flows*, to produce accurate probabilistic forecasts that are crucial for decision-makers to face the new challenges in power systems applications. Through comprehensive empirical evaluations using the open data of the Global Energy Forecasting Competition 2014, we demonstrate that our methodology is competitive with other state-of-the-art deep learning generative models: generative adversarial networks and variational autoencoders. The models producing weather-based wind, solar power, and load scenarios are properly compared both in terms of forecast value, by considering the case study of an energy retailer, and quality using several complementary metrics.

Word count: 6, 300.

Keywords: Deep learning, Normalizing flows, Energy forecasting, Time series, Generative adversarial networks, Variational autoencoders

1. Introduction

To limit climate change and achieve the ambitious targets prescribed by the Intergovernmental Panel on Climate Change [1], the transition towards a carbon-free society goes through an inevitable increase of the share of renewable generation in the energy mix. However, in contrast to conventional power plants, renewable energy is subject to uncertainty. In this context, *probabilistic forecasts* [2], which aim at modeling the distribution of all possible future realizations, have become an important tool to equip decision-makers, hopefully leading to better decisions in energy applications [3, 4, 5].

This paper focuses on *scenario generation*, a popular probabilistic forecasting method to capture the uncertainty of load, photovoltaic (PV) generation, and wind generation. It consists of producing sequences of possible load or power generation realizations for one or more locations. The density associated with the generative process is sometimes modeled by using simple parametric distributions, *e.g.*, the Weibull distribution for wind speed [6], or the beta distribution for solar irradiance [7]. In this line, the (Gaussian) copula method

has been widely used to model the spatial and temporal characteristics of wind and PV generation [8, 9]. In contrast, deep generative models such as *Variational AutoEncoders* (VAEs) [10] and *Generative Adversarial Networks* (GANs) [11] directly learn a generative process of the data. They have demonstrated their effectiveness in many applications to compute accurate probabilistic forecasts including power system applications [12, 13, 14, 15].

This study investigates the implementation of *Normalizing Flows* [16, NFs] in power system applications. NFs define a new class of probabilistic generative models that has gained increasing interest from the deep learning community in recent years. A NF learns a sequence of transformations, a *flow*, from a density known analytically, *e.g.*, a *Normal* distribution, to a complex target distribution. In contrast to other deep generative models, NFs can directly be trained by maximum likelihood estimation. They have proven to be an effective way to model complex data distributions with neural networks in many domains such as speech synthesis [17] or fundamental physics [18, 19], and have been applied in the capacity firming framework by Dumas et al. [20].

Our work goes several steps further than Ge et al. [21] that demonstrated the competitiveness of NFs

*Corresponding author

Email address: jdumas@uliege.be (Jonathan Dumas)

regarding GANs and VAEs for generating daily load profiles. First, we study the conditional version of these models to demonstrate they can take into account additional contextual information such as weather forecasts or geographical locations. Second, we extensively compare the model’s performances both in terms of forecast value and quality. The forecast quality corresponds to the ability of the forecasts to genuinely inform of future events by mimicking the characteristics of the processes involved. The forecast value relates to the benefits from using forecasts in a decision-making process such as participation in the electricity market. Third, we consider PV and wind generations in addition to load profiles. Finally, in contrast to the affine NFs used in their work, we rely on monotonic transformations which are universal density approximators [22].

The main contributions of this paper are three-fold:

1. We provide a fair comparison both in terms of quality and value with the state-of-the-art deep learning generative models, GANs and VAEs, using the open data of the Global Energy Forecasting Competition 2014 (GEFcom 2014) [23]. To the best of our knowledge it is the first study that extensively compares the NFs, GANs, and VAEs on several datasets, PV generation, wind generation, and load with a proper assessment of the quality and value based on complementary metrics, and an easily reproducible case study;
2. We implement conditional generative models to compute improved weather-based PV, wind power, and load scenarios. In contrast to most of the previous studies that focused mainly on past observations;
3. Overall, we demonstrate that NFs are more accurate both in terms of quality and value, providing further evidence for deep learning practitioners to implement this approach in more advanced power system applications.

In addition to these contributions, this study also provides open-access to the Python code¹ to help the community to reproduce the experiments. The remainder of this paper is organized as follows. Section 2 discusses the related work. Section 3 presents the generative models implemented: NFs, GANs, and VAEs. Section 4

provides the quality and value assessment methodologies. Section 5 details empirical results on the GEFcom 2014 dataset, and Section 6 summarizes the main findings and highlights ideas for further work. Appendix A provides additional information on the generative models, Appendix B details the quality metrics and the retailer energy case study formulation, and Appendix C presents additional quality results.

2. Related work

Recurrent neural networks (RNNs) are one of the most famous deep learning techniques adopted in energy forecasting applications [24, 25, 26]. Guidelines and best practices are developed by Hewamalage et al. [27] for forecasting practitioners on an extensive empirical study with an open-source software framework of existing RNN architectures. In the continuity, Toubeau et al. [28] implemented a bidirectional long short-term memory (BLSTM) architecture. It is trained using quantile regression and combined with a copula-based approach to generate scenarios. This methodology is compared with other models in terms of forecast quality and value using a scenario-based stochastic optimization case study. Finally, Salinas et al. [29] trained an autoregressive recurrent neural network on several real-world datasets producing accurate probabilistic forecasts with little or no hyper-parameter tuning.

Recently, VAEs [30, 31] and GANs [12, 32, 25, 33] have been both used to generate PV, wind power, and load scenarios. They both make probabilistic forecasts in the form of Monte Carlo samples that can be used to compute consistent quantile estimates for all sub-ranges in the prediction horizon. Thus, they cannot suffer from the issue raised by Ordiano et al. [34] on the non-differentiable quantile loss function. Improved versions of GANs and VAEs such as Wasserstein-GANs and β -VAEs have also been explored in the context of energy forecasting [35, 36, 37]. However, most of these studies did not benefit from conditional information such as weather forecasts to generate improved PV power, wind power, and load scenarios. In addition, to the best of our knowledge, only Ge et al. [21] compared NFs to these techniques for the generation of daily load profiles. Nevertheless, the comparison is only based on quality metrics, and the models do not take into account weather forecasts.

3. Background

This section formally introduces the conditional version of NFs, GANs, and VAEs implemented in this

¹It will be available at the end of the reviewing process.

study. We assume the reader is familiar with the neural network’s basics. However, for further information Goodfellow et al. [38], Zhang et al. [39] provide a comprehensive introduction to modern deep learning approaches.

3.1. Multi-output forecast

Let us consider some dataset $\mathcal{D} = \{\mathbf{x}^i, \mathbf{c}^i\}_{i=1}^N$ of N independent and identically distributed samples from the joint distribution $p(\mathbf{x}, \mathbf{c})$ of two continuous variables X and C . X being the wind generation, PV generation, or load, and C the weather forecasts. They are both composed of T periods per day, with $\mathbf{x}^i := [x_1^i, \dots, x_T^i]^\top \in \mathbb{R}^T$ and $\mathbf{c}^i := [c_1^i, \dots, c_T^i]^\top \in \mathbb{R}^T$. The goal of this work is to generate multi-output weather-based scenarios $\hat{\mathbf{x}} \in \mathbb{R}^T$ that are distributed under $p(\mathbf{x}|\mathbf{c})$.

A generative model is a probabilistic model $p_\theta(\cdot)$, with parameters θ , that can be used as a generator of the data. Its purpose is to generate synthetic but realistic data $\hat{\mathbf{x}} \sim p_\theta(\mathbf{x}|\mathbf{c})$ whose distribution is as close as possible to the unknown data distribution $p(\mathbf{x}|\mathbf{c})$. In our application, it computes on a day-ahead basis a set of M scenarios at day $d - 1$ for day d

$$\hat{\mathbf{x}}_d^i := [\hat{x}_{d,1}^i, \dots, \hat{x}_{d,T}^i]^\top \in \mathbb{R}^T \quad i = 1, \dots, M. \quad (1)$$

For the sake of clarity, we omit the indexes d and i when referring to a scenario $\hat{\mathbf{x}}$ in the following.

3.2. Deep generative models

3.2.1. Normalizing flows

A normalizing flow is defined as a sequence of invertible transformations $f_k : \mathbb{R}^T \rightarrow \mathbb{R}^T$, $k = 1, \dots, K$, composed together to create an expressive invertible mapping $f_\theta := f_1 \circ \dots \circ f_K : \mathbb{R}^T \rightarrow \mathbb{R}^T$. This composed function can be used to perform density estimation, using f_θ to map a sample $\mathbf{x} \in \mathbb{R}^T$ onto a latent vector $\mathbf{z} \in \mathbb{R}^T$ equipped with a known and tractable probability density function p_z , e.g., a Normal distribution. The transformation f_θ implicitly defines a density $p_\theta(\mathbf{x})$ that is given by the change of variables

$$p_\theta(\mathbf{x}) = p_z(f_\theta(\mathbf{x})) |\det J_{f_\theta}(\mathbf{x})|, \quad (2)$$

where J_{f_θ} is the Jacobian of f_θ regarding \mathbf{x} . The model is trained by maximizing the log-likelihood $\sum_{i=1}^N \log p_\theta(\mathbf{x}^i, \mathbf{c}^i)$ of the model’s parameters θ given the dataset \mathcal{D} . For simplicity let us assume a single-step flow f_θ to drop the index k for the rest of the discussion.

In general, f_θ can take any form as long as it defines a bijection. However, a common solution to make the Jacobian computation tractable in (2) consists of implementing an *autoregressive* transformation [40], i.e.,

such that f_θ can be rewritten as a vector of scalar bijections f^i

$$f_\theta(\mathbf{x}) := [f^1(x_1; h^1), \dots, f^T(x_T; h^T)]^\top, \quad (3a)$$

$$h^i := h^i(\mathbf{x}_{<i}; \varphi^i) \quad 2 \leq i \leq T, \quad (3b)$$

$$\mathbf{x}_{<i} := [x_1, \dots, x_{i-1}]^\top \quad 2 \leq i \leq T, \quad (3c)$$

$$h^1 \in \mathbb{R}, \quad (3d)$$

where $f^i(\cdot; h^i) : \mathbb{R} \rightarrow \mathbb{R}$ is partially parameterized by an autoregressive conditioner $h^i(\cdot; \varphi^i) : \mathbb{R}^{i-1} \rightarrow \mathbb{R}^{h^i}$ with parameters φ^i , and θ the union of all parameters φ^i .

There is a large choice of transformers f^i : affine, non-affine, integration-based, etc. In this work, an integration-based transformer is implemented by using the class of Unconstrained Monotonic Neural Networks (UMNN) proposed by Wehenkel and Louppe [41], which have been demonstrated to be a universal density approximator of continuous random variables when combined with autoregressive functions. The UMNN consists of a neural network architecture that enables learning arbitrary monotonic functions. It is achieved by parameterizing the bijection f^i as follows

$$f^i(x_i; h^i) = \int_0^{x_i} \tau^i(x_i, h^i) dt + \beta^i(h^i), \quad (4)$$

where $\tau^i(\cdot; h^i) : \mathbb{R}^{h^i+1} \rightarrow \mathbb{R}^+$ is the integrand neural network with a strictly positive scalar output, $h^i \in \mathbb{R}^{h^i}$ an embedding made by the conditioner, and $\beta^i(\cdot) : \mathbb{R}^{h^i} \rightarrow \mathbb{R}$ a neural network with a scalar output. The forward evaluation of f^i requires solving the integral (4) and is efficiently approximated numerically by using the Clenshaw-Curtis quadrature. The pseudo-code of the forward and backward passes is provided by Wehenkel and Louppe [41].

Papamakarios et al. [42]’s Masked Autoregressive Network (MAF) is implemented to simultaneously parameterize the T autoregressive embeddings h^i of the flow (3). Then, the change of variables formula applied to the UMMN-MAF transformation results in the following log-density when considering weather forecasts

$$\log p_\theta(\mathbf{x}, \mathbf{c}) = \log p_z(f_\theta(\mathbf{x}, \mathbf{c})) |\det J_{f_\theta}(\mathbf{x}, \mathbf{c})|, \quad (5a)$$

$$= \log p_z(f_\theta(\mathbf{x}, \mathbf{c})) + \sum_{i=1}^T \log \tau^i(x_i, h^i(\mathbf{x}_{<i}, \mathbf{c})), \quad (5b)$$

that can be computed exactly and efficiently with a single forward pass. The UMNN-MAF approach implemented, illustrated by Figure 1, is referred to as NF in the rest of the paper. Appendix A.1 provides additional information on NFs.

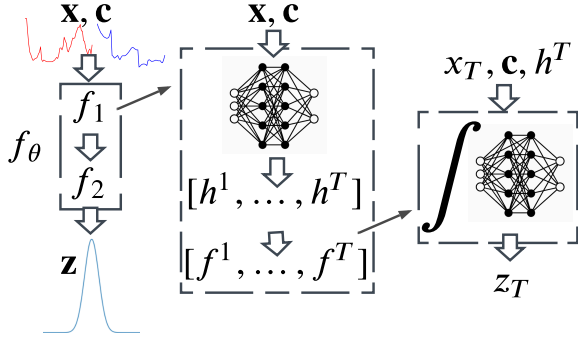


Figure 1: Conditional UMNN-MAF.

3.2.2. Variational autoencoders

A VAE is a deep latent variable model composed of an *encoder* and a *decoder* which are jointly trained to maximize a lower bound on the likelihood. The encoder $q_\varphi(\cdot) : \mathbb{R}^T \times \mathbb{R}^{|\mathcal{C}|} \rightarrow \mathbb{R}^d$ approximates the intractable posterior $p(\mathbf{z}|\mathbf{x}, \mathbf{c})$, and the decoder $p_\theta(\cdot) : \mathbb{R}^d \times \mathbb{R}^{|\mathcal{C}|} \rightarrow \mathbb{R}^T$ the likelihood $p(\mathbf{x}|\mathbf{z}, \mathbf{c})$ with $\mathbf{z} \in \mathbb{R}^d$. Maximum likelihood is intractable as it would require marginalizing with respect to all possible realizations of the latent variables \mathbf{z} . Kingma and Welling [10] addressed this issue by maximizing the *variational lower bound* $\mathcal{L}_{\theta, \varphi}(\mathbf{x}, \mathbf{c})$ as follows

$$\log p_\theta(\mathbf{x}|\mathbf{c}) = \text{KL}[q_\varphi(\mathbf{z}|\mathbf{x}, \mathbf{c}) \| p(\mathbf{z}|\mathbf{x}, \mathbf{c})] + \mathcal{L}_{\theta, \varphi}(\mathbf{x}, \mathbf{c}), \quad (6a)$$

$$\geq \mathcal{L}_{\theta, \varphi}(\mathbf{x}, \mathbf{c}), \quad (6b)$$

$$\mathcal{L}_{\theta, \varphi}(\mathbf{x}, \mathbf{c}) := \mathbb{E}_{q_\varphi(\mathbf{z}|\mathbf{x}, \mathbf{c})} \left[\log \frac{p(\mathbf{z})p_\theta(\mathbf{x}|\mathbf{z}, \mathbf{c})}{q_\varphi(\mathbf{z}|\mathbf{x}, \mathbf{c})} \right], \quad (6c)$$

as the Kullback-Leibler (KL) divergence [43] is non-negative. Appendix A.2 details how to compute the gradients of $\mathcal{L}_{\theta, \varphi}(\mathbf{x}, \mathbf{c})$, and its exact expression for the implemented VAE composed of fully connected neural networks for both the encoder and decoder, depicted in Figure 2.

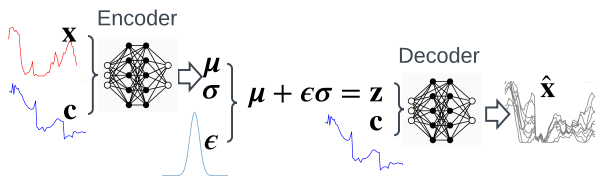


Figure 2: Conditional VAE.

3.2.3. Generative adversarial networks

GANs are a class of deep generative models proposed by Goodfellow et al. [11] where the key idea is the ad-

versarial training of two neural networks, the *generator* and the *discriminator*, during which the generator learns iteratively to produce realistic scenarios until they cannot be distinguished anymore by the discriminator from real data. The generator $g_\theta(\cdot) : \mathbb{R}^d \times \mathbb{R}^{|\mathcal{C}|} \rightarrow \mathbb{R}^T$ maps a latent vector $\mathbf{z} \in \mathbb{R}^d$ equipped with a known and tractable prior probability density function $p(\mathbf{z})$, e.g., a Normal distribution, onto a sample $\mathbf{x} \in \mathbb{R}^T$, and is trained to fool the discriminator. The discriminator $d_\phi(\cdot) : \mathbb{R}^T \times \mathbb{R}^{|\mathcal{C}|} \rightarrow [0, 1]$ is a classifier trained to distinguish between true samples \mathbf{x} and generated samples $\hat{\mathbf{x}}$. Goodfellow et al. [11] demonstrated that solving the following min-max problem

$$\theta^* = \arg \min_{\theta} \max_{\phi} V(\phi, \theta), \quad (7)$$

where $V(\phi, \theta)$ is the value function, recovers the data generating distribution if $g_\theta(\cdot)$ and $d_\phi(\cdot)$ are given enough capacity. The state-of-the-art conditional Wasserstein GAN with gradient penalty (WGAN-GP) proposed by Gulrajani et al. [44] is implemented with $V(\phi, \theta)$ defined as

$$V(\phi, \theta) = - \left(\mathbb{E}_{\tilde{\mathbf{x}}} [d_\phi(\tilde{\mathbf{x}}|\mathbf{c})] - \mathbb{E}_{\mathbf{x}} [d_\phi(\mathbf{x}|\mathbf{c})] + \lambda \text{GP} \right), \quad (8a)$$

$$\text{GP} = \mathbb{E}_{\tilde{\mathbf{x}}} \left[\left(\|\nabla_{\tilde{\mathbf{x}}} d_\phi(\tilde{\mathbf{x}}|\mathbf{c})\|_2 - 1 \right)^2 \right], \quad (8b)$$

where $\tilde{\mathbf{x}}$ is implicitly defined by sampling convex combinations between the data and the generator distributions $\tilde{\mathbf{x}} = \rho \hat{\mathbf{x}} + (1-\rho)\mathbf{x}$ with $\rho \sim \mathcal{U}(0, 1)$. The WGAN-GP constrains the gradient norm of the discriminator's output with respect to its input, to enforce the 1-Lipschitz conditions, in contrast to the weight clipping of WGAN that sometimes generates only poor samples or fails to converge. Appendix A.3 details the successive improvements from the original GAN to the WGAN, and the final WGAN-GP implemented, referred to as GAN in the rest of the paper, depicted in Figure 3.

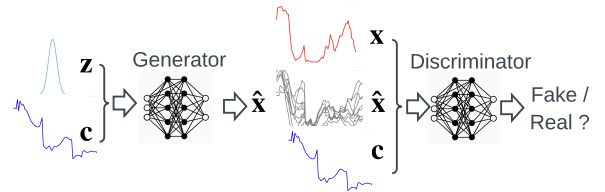


Figure 3: Conditional WGAN-GP.

4. Value and quality assessment

For predictions in any form, one must differentiate between their quality and their value [3]. Forecast qual-

ity corresponds to the ability of the forecasts to genuinely inform of future events by mimicking the characteristics of the processes involved. Forecast value relates, instead, to the benefits from using forecasts in a decision-making process such as participation in the electricity market.

4.1. Forecast quality

In total six complementary quality metrics are combined to conduct a relevant quality analysis. They can be divided in two groups, the *common* metrics composed of the continuous rank probability score, the quantile score, and the reliability diagram, and the *specific* metrics composed of a classifier-based metric, the correlation matrix between scenarios for a given context, and the Diebold and Mariano test.

Common metrics

The continuous rank probability score (CRPS) [45] penalizes the lack of resolution of the predictive distributions as well as biased forecasts. It is negatively oriented, *i.e.*, the lower, the better, and for deterministic forecasts, it turns out to be the mean absolute error (MAE). The CRPS is selected to quantitatively assess the performance of the generative methods similar to the MAE when considering point forecasts.

The quantile score (QS), also known as the pinball loss score, is complementary to the CRPS as it permits obtaining detailed information about the forecast quality at specific probability levels, *i.e.*, over-forecasting or under-forecasting, and particularly those related to the tails of the predictive distribution [46]. It is negatively oriented and assigns asymmetric weights to negative and positive errors for each quantile. Appendix B.1 presents the definitions of the CRPS, the QS.

Finally, the reliability diagram is a graphical verification used to evaluate the reliability of the quantiles derived from the scenarios. Quantile forecasts are reliable if their nominal proportions are equal to the proportions of the observed value.

Specific metrics

A conditional classifier-based scoring rule is designed by implementing an Extra-Trees classifier [47] to discriminate true from generated samples. The receiver operating characteristic (ROC) curves are computed for each generative model on the testing set. The best generative model should achieve an area under the ROC curve (AUC) of 0.5, *i.e.*, each sample is equally likely to be predicted as true or false meaning the classifier is unable to discriminate generated scenarios from the true observations.

The second specific metric consists of computing the correlation matrix between the scenarios generated for given weather forecasts. Formally, let $\{\hat{\mathbf{x}}^i\}_{i=1}^M$ be the set of M scenarios generated for a given day of the testing set. It is a matrix ($M \times 24$) where each row is a scenario. Then, the Pearson's correlation coefficients are computed into a correlation matrix (24×24). This metric indicates the variety of scenario shapes.

Finally, the Diebold-Mariano (DM) test [48] is used as a significance test for both the CRPS and QS metrics. Indeed, when different models have almost identical values in the selected error measures, it is difficult to draw statistically significant conclusions on the out-performance of the forecasts of one model by those of another. The multivariate variant of the DM test is implemented following Ziel and Weron [49], where only one statistic for each pair of models is computed based on the 24-dimensional vector of errors for each day. Appendix B.1 provides additional information on the classifier-based metric, and the DM test.

4.2. Forecast value

A model that yields lower errors in terms of forecast quality may not always point to a more effective model for forecast practitioners [5]. To this end, similarly to [28], the forecast value is assessed by considering the day-ahead market scheduling of electricity aggregators, such as energy retailers or generation companies. The energy retailer aims to balance its portfolio on an hourly basis, to avoid financial penalties in case of imbalance, by exchanging the surplus or deficit of energy in the day-ahead electricity market. The energy retailer may have a battery energy storage system (BESS) to manage its portfolio and to minimize imports from the main grid when day-ahead prices are prohibitive.

Let e_t [MWh] be the net energy retailer position on the day-ahead market during the t -th hour of the day, which is modeled as a first stage variable. Let y_t [MWh] be the realized net energy retailer position during the t -th hour of the day, which is modeled as a second stage variable due to the stochastic processes of the PV generation, wind generation, and load. Let π_t [€/MWh] the clearing price in the spot day-ahead market for the t -th hour of the day, q_t ex-post settlement price for negative imbalance $y_t < e_t$, and λ_t ex-post settlement price for positive imbalance $y_t > e_t$. The energy retailer is assumed to be a price taker in the day-ahead market. This is motivated by the fact that the individual energy retailer capacity is negligible relative to the whole market. The forward settlement price π_t is assumed to be fixed and known. As imbalance prices tend to exhibit volatility and are difficult to forecast, they are modeled as ran-

dom variables, with expectations denoted by $\bar{q}_t = \mathbb{E}[q_t]$ and $\bar{\lambda}_t = \mathbb{E}[\lambda_t]$. They are assumed to be independent random variables from the energy retailer portfolio.

A stochastic planner with a linear programming formulation and linear constraints is implemented using a scenario-based approach. The planner computes the day-ahead bids e_t that cannot be modified in the future when the uncertainty is resolved. The second stage corresponds to the dispatch decisions $y_{t,\omega}$ in scenario ω that aims at avoiding portfolio imbalances modeled by a cost function f^c . The second-stage decisions are therefore scenario-dependent and can be adjusted according to the realization of the stochastic parameters. The stochastic planner objective to maximize is

$$J_S = \mathbb{E} \left[\sum_{t \in \mathcal{T}} \pi_t e_t + f^c(e_t, y_{t,\omega}) \right], \quad (9)$$

where the expectation is taken with respect to the random variables that are the PV generation, wind generation, and load. Using a scenario-based approach, (9) is approximated by

$$J_S \approx \sum_{\omega \in \Omega} \alpha_\omega \sum_{t \in \mathcal{T}} \left[\pi_t e_t + f^c(e_t, y_{t,\omega}) \right], \quad (10)$$

with α_ω the probability of scenario $\omega \in \Omega$, and $\sum_{\omega \in \Omega} \alpha_\omega = 1$. The optimization problem is detailed in [Appendix B.2](#).

5. Numerical Results

The quality and value evaluations of the models are conducted on the load, wind, and PV tracks of the open-access GEFCom 2014 dataset [23], composed of one, ten, and three zones, respectively.

5.1. Implementation details

By appropriate normalization, we standardize the weather forecasts to have a zero mean and unit variance. Table 1 provides a summary of the implementation details described in what follows. For the sake of proper model training and evaluation, the dataset is divided into three parts per track considered: learning, validation, and testing sets. The learning set (LS) is used to fit the models, the validation set (VS) to select the optimal hyper-parameters, and the testing set (TS) to assess the forecast quality and value. The number of samples (#), expressed in days, of the VS and TS is $50 \cdot n_z$, with n_z the number of zones of the track considered. The 50 days are selected randomly from the dataset, and the learning set is composed of the remaining part with $D \cdot n_z$ samples, where D is provided for each track in Table 1. The

NF, VAE, and GAN use the weather forecasts as inputs to generate on a day-ahead basis M scenarios $\hat{\mathbf{x}} \in \mathbb{R}^T$. The hyper-parameters values used for the experiments are provided in [Appendix A.4](#).

Wind track

The zonal \mathbf{u}^{10} , \mathbf{u}^{100} and meridional \mathbf{v}^{10} , \mathbf{v}^{100} wind components at 10 and 100 meters are selected, and six features are derived following the formulas provided by [50] to compute the wind speed \mathbf{ws}^{10} , \mathbf{ws}^{100} , energy \mathbf{we}^{10} , \mathbf{we}^{100} and direction \mathbf{wd}^{10} , \mathbf{wd}^{100} at 10 and 100 meters

$$\mathbf{ws} = \sqrt{\mathbf{u} + \mathbf{v}}, \quad (11a)$$

$$\mathbf{we} = \frac{1}{2} \mathbf{ws}^3, \quad (11b)$$

$$\mathbf{wd} = \frac{180}{\pi} \arctan(\mathbf{u}, \mathbf{v}). \quad (11c)$$

For each generative model, the wind zone is taken into account with one hot-encoding variable Z_1, \dots, Z_{10} , and the wind feature input vector for a given day d is

$$\mathbf{c}_d^{\text{wind}} = [\mathbf{u}_d^{10}, \mathbf{u}_d^{100}, \mathbf{v}_d^{10}, \mathbf{v}_d^{100}, \mathbf{ws}_d^{10}, \mathbf{ws}_d^{100}, \mathbf{we}_d^{10}, \mathbf{we}_d^{100}, \mathbf{wd}_d^{10}, \mathbf{wd}_d^{100}, Z_1, \dots, Z_{10}], \quad (12)$$

of dimension $n_f \cdot T + n_z = 10 \cdot 24 + 10$.

PV track

The solar irradiation \mathbf{I} , the air temperature \mathbf{T} , and the relative humidity \mathbf{rh} are selected, and two features are derived by computing \mathbf{I}^2 and \mathbf{IT} . For each generative model, the PV zone is taken into account with one hot-encoding variable Z_1, Z_2, Z_3 , and the PV feature input vector for a given day d is

$$\mathbf{c}_d^{\text{PV}} = [\mathbf{I}_d, \mathbf{T}_d, \mathbf{rh}_d, \mathbf{I}_d^2, \mathbf{IT}_d, Z_1, Z_2, Z_3], \quad (13)$$

of dimension $n_f \cdot T + n_z$. For practical reasons, the periods where the PV generation is always 0, across all zones and days, are removed, and the final dimension of the input feature vector is $n_f \cdot T + n_z = 5 \cdot 16 + 3$.

Load track

The 25 weather station temperature $\mathbf{w}_1, \dots, \mathbf{w}_{25}$ forecasts are used. There is only one zone, and the load feature input vector for a given day d is

$$\mathbf{c}_d^{\text{load}} = [\mathbf{w}_1, \dots, \mathbf{w}_{25}], \quad (14)$$

of dimension $n_f \cdot T = 25 \cdot 24$.

	Wind	PV	Load
T periods	24	16	24
n_z zones	10	3	—
n_f features	10	5	25
\mathbf{c}_d dimension	$n_f \cdot T + n_z$	$n_f \cdot T + n_z$	$n_f \cdot T$
# LS (days)	$631 \cdot n_z$	$720 \cdot n_z$	1999
# VS/TS (days)	$50 \cdot n_z$	$50 \cdot n_z$	50

Table 1: Dataset and implementation details.

5.2. Quality results

A thorough comparison of the models is conducted on the wind track, and [Appendix C](#) provides the Figures of the other tracks for the sake of clarity. Note that the model ranking slightly differs depending on the track.

Wind track

In addition to the generative models, a naive approach is designed (RAND), where the scenarios of the learning, validation, and testing sets are sampled randomly from the learning, validation, and testing sets, respectively. Intuitively, it boils down to assume that past observations are repeated. These scenarios are realistic but may not be compatible with the context. Each model generates a set of 100 scenarios for each day of the testing set. Figure 4 compares the QS, reliability diagram, and CRPS of the wind (markers), PV (plain), and load (dashed) tracks. Overall, for the wind track in terms of CRPS, QS, and reliability diagrams the VAE achieves slightly better scores, then followed by the NF, and the GAN.

Figures 5a and 5b provide the results of the multivariate DM test for the CRPS and QS, respectively. The heat map indicates the range of the p -values, the closer they are to zero, dark green, the more significant the difference between the scores of two models for a given metric. The statistical threshold is set to 5 % but the scale color is capped at 10 % for a better exposition of the relevant results. For instance, when considering the DM test for the RAND CRPS, all the columns of the RAND row are in dark green indicating that the RAND scenarios are always significantly outperformed by the other models. The multivariate DM test confirms the VAE generates the best scenarios for the wind track followed by the NF that is only outperformed by the VAE, and the GAN outperformed by both the VAE and NF.

These results are consistent with the classifier-based metric depicted in Figure 5c, where the VAE is the best

to mislead the classifier followed by the NF, and GAN. However, the left part of Figure 6 indicates the shape of the scenarios differs significantly between the models as NF scenarios are more variable for a given context. The VAE and GAN scenarios seem to have a similar shape and differ mainly with a vertical translation. It is confirmed by the corresponding correlation matrices, provided by the right part of Figure 6 demonstrating there is no correlation between NF scenarios. On the contrary, the VAE and GAN correlation matrices tend to be similar.

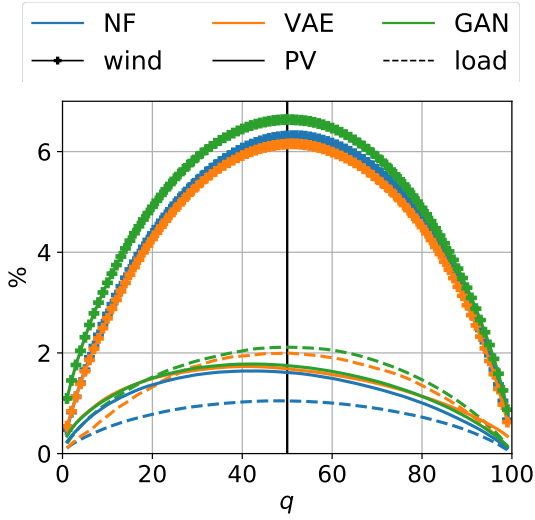
All tracks

Table 2 provides the averaged quality scores where the CRPS is averaged over the 24 time periods $\overline{\text{CRPS}}$, the QS over the 99 percentiles $\overline{\text{QS}}$, MAE-r is the mean absolute error between the reliability curve and the diagonal, and $\overline{\text{AUC}}$ is the mean of the 50 AUC. Overall, for

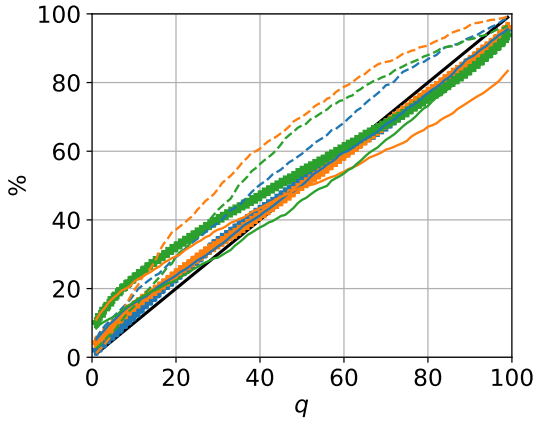
		$\overline{\text{CRPS}}$	$\overline{\text{QS}}$	MAE-r	$\overline{\text{AUC}}$
(a)	NF	9.07	4.58	2.83	0.933
	VAE	8.80	4.45	2.67	0.871
	GAN	9.79	4.95	6.82	0.971
	RAND	16.92	8.55	1.01	0.916
(b)	NF	2.35	1.19	2.66	0.946
	VAE	2.60	1.31	9.04	0.968
	GAN	2.61	1.32	4.94	0.996
	RAND	4.92	2.48	3.94	0.945
(c)	NF	1.51	0.76	7.70	0.820
	VAE	2.74	1.39	13.97	0.848
	GAN	3.01	1.52	9.99	0.999
	RAND	6.74	3.40	0.88	0.945

Table 2: Averaged quality scores (a) wind, (b) PV, and (c) load. The best performing deep learning generative model for each track is written in bold.

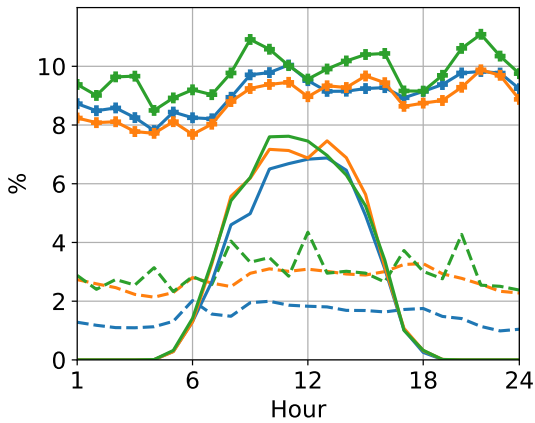
both the PV and load tracks in terms of CRPS, QS, and reliability diagrams, the NF outperforms the VAE and GAN and is slightly outperformed by the VAE on the wind track. These results are confirmed by the multivariate DM test where the NF scenarios of both the load and PV tracks are the best as depicted in Figure C.8, then followed by the VAE, and the GAN. The classifier-based metric results for both the load and PV tracks, provided by Figure C.8, confirm this trend where the NF is the best to trick the classifier followed by the VAE, and GAN.



(a) Quantile score.



(b) Reliability diagram.



(c) CRPS.

Figure 4: Quality common metrics comparison on the wind (markers), PV (plain), and load (dashed) tracks.

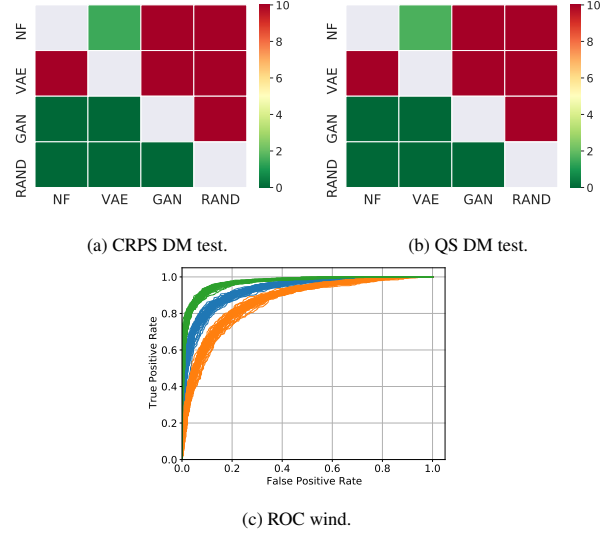


Figure 5: Wind track DM tests and classifier-based metric.

Similar to the wind track, the shape of the scenarios differs significantly between the NF and the other models for both the load and PV tracks as indicated by the left part of Figures C.9 and C.10, and the corresponding correlation matrices provided by the right part of Figures C.9 and C.10. Note the load track scenarios are highly correlated for both the VAE and GAN. This difference between the NF and the other generative model may be explicated by the design of the methods. The NF learns explicitly the probability density function (PDF) of the multi-dimensional random variable considered. Thus, the NF scenarios are generated according to the learned PDF producing multiple shapes of scenarios. In contrast, the generator of the GAN is trained to fool the discriminator, and it may find a shape particularly efficient leading to a set of similar scenarios. Concerning the VAE, it is less obvious, but by design, the decoder is trained to generate scenarios from the latent space assumed to follow a Gaussian distribution that may lead to less variability.

5.3. Value results

The retailer portfolio is composed of wind and PV generation, and load. The 50 days of the testing set are used and combined with the 30 possible PV and wind generation zones, resulting in 1 500 independent simulated days. Figure 7 illustrates an arbitrary random day of the testing set with the first zone for both the PV and wind. π_t [€/ MWh] is the day-ahead prices on February 6, 2020 of the Belgian day-ahead market used for the 1 500 days simulated. The negative \bar{q}_t and

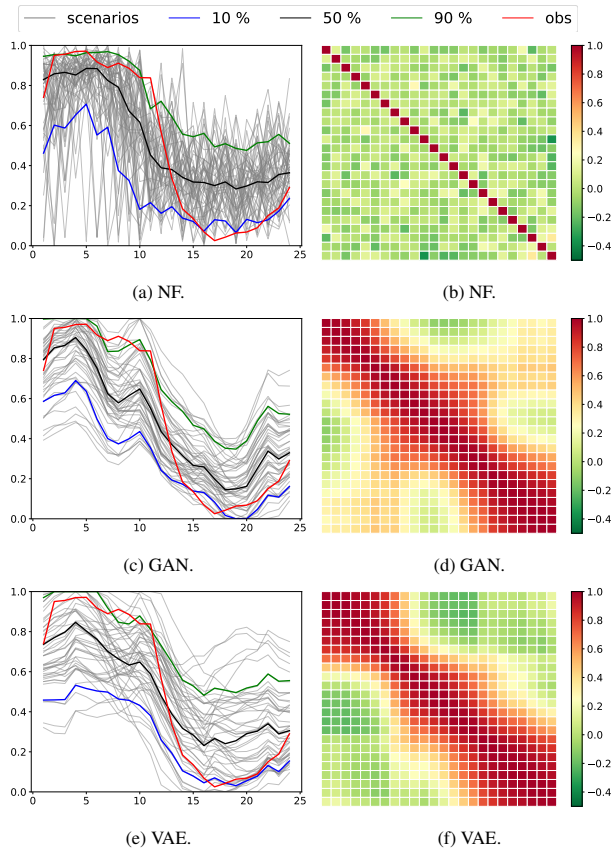


Figure 6: Left part: 50 wind scenarios (grey) of a randomly selected day of the testing set along with the 10 %, 50 %, and 90 % quantiles, and the observations in red (obs). Right part: corresponding correlation matrices.

positive $\bar{\lambda}_t$ imbalance prices are set to $2 \times \pi_t, \forall t \in \mathcal{T}$. The retailer aims to balance the net power, red curve in Figure 7, by importing/exporting from/to the main grid. Usually, the net is positive (negative) at noon (evening) when the PV generation is maximal (minimal) and the load is minimal (maximal). As the day-ahead spot price is often maximal during the evening load peak, the retailer seeks to save power during the day by charging the battery to decrease the import during the evening. Therefore, the more accurate the PV, wind generation, and load scenarios are, the better is the day-ahead planning.

The battery minimum s^{\min} and maximum s^{\max} capacities are 0 and 1, respectively. It is assumed to be capable of fully (dis)charging in two hours with $y_{\max}^{\text{dis}} = y_{\max}^{\text{cha}} = s^{\max}/2$, and the (dis)charging efficiencies are $\eta^{\text{dis}} = \eta^{\text{cha}} = 95\%$. Each simulation day is independent with a fully discharged battery at the first and last period of each day $s^{\text{ini}} = s^{\text{end}} = 0$. The 1 500 stochastic

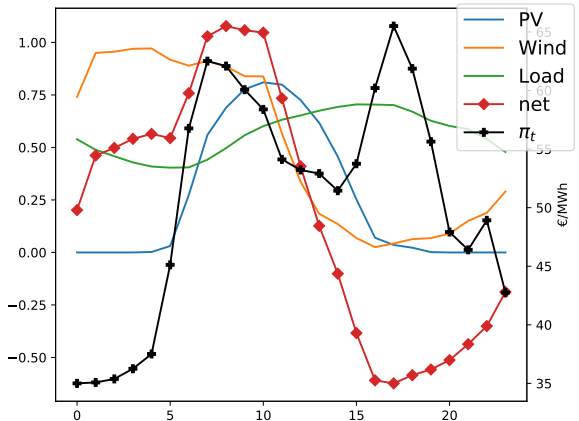


Figure 7: An arbitrary random day of the testing set with the first zone for both the PV and wind. The day-ahead prices π_t on February 6, 2020 of the Belgian day-ahead market.

optimization problems are solved with 50 PV, wind generation, and load scenarios. The python Gurobi library is used to implement the algorithms in Python 3.7, and Gurobi² 9.0.2 is used to solve the optimization problems. Numerical experiments are performed on an Intel Core i7-8700 3.20 GHz based computer with 12 threads and 32 GB of RAM running on Ubuntu 18.04 LTS.

The net profit, that is the profit minus penalty, is computed for the 1 500 days of the simulation and aggregated in the first row of Table 3. The ranking of each model is computed for the 1 500 days, and the cumulative ranking is expressed in terms of percentage in Table 3. NF outperformed both the GAN and VAE with a total net profit of 107 k€. There is still room for improvement as the oracle, which has perfect knowledge of the future, achieved 300 k€. NF, ranked first 39.0 % during the 1 500 simulation days and achieved the first and second ranks 69.6 %. Overall, in terms of

	NF	VAE	GAN
Net profit (k€)	107	97	93
1 (%)	39.0	31.8	29.2
1 & 2 (%)	69.6	68.3	62.1
1 & 2 & 3 (%)	100	100	100

Table 3: Total net profit (k€) and cumulative ranking (%).

forecast value, the NF outperforms the VAE and GAN.

²<https://www.gurobi.com/>

However, this case study is "simple" and stochastic optimization relies mainly on the quality of the average of the scenarios. Therefore, one may consider taking advantage of the particularities of a specific method by considering more advanced case studies. In particular, the specificity of the NFs to provide direct access to the probability density function may be of great interest in specific applications. This is left for future investigations as such more advanced case studies would prevent a fair comparison between models.

6. Conclusion

This paper proposed a fair and thorough comparison of NFs with the state-of-the-art deep learning generative models, GANs and VAEs, both in terms of quality and value. The experiments were performed by using the open data of the Global Energy Forecasting Competition 2014, where the generative models use the conditional information to compute improved weather-based PV power, wind power, and load scenarios. This study demonstrated that NFs are capable of challenging GANs and VAEs as they are, overall, more accurate both in terms of quality and value, and can be used effectively by non-expert deep learning practitioners. In addition, NFs have several advantages over more traditional deep learning approaches that should motivate their introduction into power system applications:

- (i) NFs directly learn the stochastic multivariate distribution of the underlying process by maximizing the likelihood. Therefore, in contrast to VAEs and GANs, NFs provide access to the exact likelihood of the model's parameters, hence offering a sound and direct way to optimize the network parameters [51]. It may open a new range of advanced applications benefiting from this advantage. For instance, to transfer scenarios from one location to another based on the knowledge of the probability density function. A second application is the importance sampling for stochastic optimization based on a scenario approach. Indeed, NFs provide for each generated scenario its likelihood making it possible to filter relevant scenarios to be used in stochastic optimization.
- (ii) In our opinion, NFs are easier to use by non-expert deep learning practitioners, once the libraries are available, as they are more reliable and robust in terms of hyper-parameters selection. GANs and VAEs are particularly sensitive to the latent space dimension, the structure of the neural networks,

the learning rate, etc. GANs convergence, by design, is unstable, and for a given set of hyper-parameters, the scenario's quality may differ completely. In contrast, it was easier to retrieve relevant NFs hyper-parameters by testing manually a few sets of values that led to satisfying training convergence and quality results.

Yet, their usage as a base component of the machine learning toolbox is still limited in comparison to GANs or VAEs.

7. Acknowledgments

The authors would like to acknowledge the authors and contributors of the Scikit-Learn [52] and Pytorch [53] Python libraries. Antoine Wehenkel is a recipient of an F.R.S.-FNRS fellowship and acknowledges the financial support of the FNRS (Belgium). Antonio Sutera is supported via the Energy Transition Funds project EPOC 2030-2050 organized by the FPS economy, S.M.E.s, Self-employed and Energy.

References

- [1] M. Allen, P. Antwi-Agyei, F. Aragon-Durand, M. Babiker, P. Bertoldi, M. Bind, S. Brown, M. Buckeridge, I. Camilloni, A. Cartwright, et al., Technical Summary: Global warming of 1.5° C. An IPCC Special Report on the impacts of global warming of 1.5° C above pre-industrial levels and related global greenhouse gas emission pathways, in the context of strengthening the global response to the threat of climate change, sustainable development, and efforts to eradicate poverty, Technical Report, Intergovernmental Panel on Climate Change, 2019.
- [2] T. Gneiting, M. Katzfuss, Probabilistic forecasting, *Annual Review of Statistics and Its Application* 1 (2014) 125–151.
- [3] J. M. Morales, A. J. Conejo, H. Madsen, P. Pinson, M. Zugno, Integrating renewables in electricity markets: operational problems, volume 205, Springer Science & Business Media, 2013.
- [4] T. Hong, S. Fan, Probabilistic electric load forecasting: A tutorial review, *International Journal of Forecasting* 32 (2016) 914–938.
- [5] T. Hong, P. Pinson, Y. Wang, R. Weron, D. Yang, H. Zareipour, et al., Energy forecasting: A review and outlook, Technical Report, Department of Operations Research and Business Intelligence, Wrocław . . . , 2020.
- [6] S. H. Karaki, B. A. Salim, R. B. Chedid, Probabilistic model of a two-site wind energy conversion system, *IEEE Transactions on Energy Conversion* 17 (2002) 530–536.
- [7] S. Karaki, R. Chedid, R. Ramadan, Probabilistic performance assessment of autonomous solar-wind energy conversion systems, *IEEE Transactions on energy conversion* 14 (1999) 766–772.
- [8] P. Pinson, H. Madsen, H. A. Nielsen, G. Papaefthymiou, B. Klöckl, From probabilistic forecasts to statistical scenarios of short-term wind power production, *Wind Energy: An International Journal for Progress and Applications in Wind Power Conversion Technology* 12 (2009) 51–62.

- [9] H. Zhang, Z. Lu, W. Hu, Y. Wang, L. Dong, J. Zhang, Coordinated optimal operation of hydro-wind-solar integrated systems, *Applied Energy* 242 (2019) 883–896.
- [10] D. P. Kingma, M. Welling, Auto-encoding variational bayes, *arXiv preprint arXiv:1312.6114* (2013).
- [11] I. J. Goodfellow, J. Pouget-Abadie, M. Mirza, B. Xu, D. Warde-Farley, S. Ozair, A. Courville, Y. Bengio, Generative adversarial networks, *arXiv preprint arXiv:1406.2661* (2014).
- [12] C. Jiang, Y. Mao, Y. Chai, M. Yu, S. Tao, Scenario generation for wind power using improved generative adversarial networks, *IEEE Access* 6 (2018) 62193–62203.
- [13] Y. Chen, P. Li, B. Zhang, Bayesian renewables scenario generation via deep generative networks, in: 2018 52nd Annual Conference on Information Sciences and Systems (CISS), IEEE, 2018, pp. 1–6.
- [14] C. Jiang, Y. Mao, Y. Chai, M. Yu, Day-ahead renewable scenario forecasts based on generative adversarial networks, *International Journal of Energy Research* (2020).
- [15] R. Yuan, B. Wang, Z. Mao, J. Watada, Multi-objective wind power scenario forecasting based on pg-gan, *Energy* (2021) 120379.
- [16] D. Rezende, S. Mohamed, Variational inference with normalizing flows, in: *International Conference on Machine Learning*, PMLR, 2015, pp. 1530–1538.
- [17] A. Oord, Y. Li, I. Babuschkin, K. Simonyan, O. Vinyals, K. Kavukcuoglu, G. Driessche, E. Lockhart, L. Cobo, F. Stimberg, et al., Parallel wavenet: Fast high-fidelity speech synthesis, in: *International conference on machine learning*, PMLR, 2018, pp. 3918–3926.
- [18] M. S. Albergo, D. Boyda, D. C. Hackett, G. Kanwar, K. Cranmer, S. Racanière, D. J. Rezende, P. E. Shanahan, Introduction to normalizing flows for lattice field theory, *arXiv preprint arXiv:2101.08176* (2021).
- [19] S. R. Green, J. Gair, Complete parameter inference for gw150914 using deep learning, *arXiv preprint arXiv:2008.03312* (2020).
- [20] J. Dumas, C. Cointe, A. Wehenkel, A. Suter, X. Fettweis, B. Cornélusse, A probabilistic forecast-driven strategy for a risk-aware participation in the capacity firming market, 2021. Manuscript submitted for publication to *IEEE Transactions on Sustainable Energy*.
- [21] L. Ge, W. Liao, S. Wang, B. Bak-Jensen, J. R. Pillai, Modeling daily load profiles of distribution network for scenario generation using flow-based generative network, *IEEE Access* 8 (2020) 77587–77597.
- [22] C.-W. Huang, D. Krueger, A. Lacoste, A. Courville, Neural autoregressive flows, in: *International Conference on Machine Learning*, PMLR, 2018, pp. 2078–2087.
- [23] T. Hong, P. Pinson, S. Fan, H. Zareipour, A. Troccoli, R. J. Hyndman, Probabilistic energy forecasting: Global energy forecasting competition 2014 and beyond, 2016.
- [24] H. Shi, M. Xu, R. Li, Deep learning for household load forecasting—a novel pooling deep rnn, *IEEE Transactions on Smart Grid* 9 (2017) 5271–5280.
- [25] Y. Chen, Y. Wang, D. Kirschen, B. Zhang, Model-free renewable scenario generation using generative adversarial networks, *IEEE Transactions on Power Systems* 33 (2018) 3265–3275.
- [26] J. Dumas, X. Fettweis, B. Cornélusse, et al., Deep learning-based multi-output quantile forecasting of PV generation, 2021. (in press in proceedings of 2021 IEEE Madrid PowerTech).
- [27] H. Hewamalage, C. Bergmeir, K. Bandara, Recurrent neural networks for time series forecasting: Current status and future directions, *International Journal of Forecasting* 37 (2020) 388–427.
- [28] J.-F. Toubeau, J. Bottieau, F. Vallée, Z. De Grève, Deep learning-based multivariate probabilistic forecasting for short-term scheduling in power markets, *IEEE Transactions on Power Systems* 34 (2018) 1203–1215.
- [29] D. Salinas, V. Flunkert, J. Gasthaus, T. Januschowski, DeepAR: Probabilistic forecasting with autoregressive recurrent networks, *International Journal of Forecasting* 36 (2020) 1181–1191.
- [30] H. Zhanga, W. Hua, R. Yub, M. Tangb, L. Dingc, Optimized operation of cascade reservoirs considering complementary characteristics between wind and photovoltaic based on variational auto-encoder, in: *MATEC Web of Conferences*, volume 246, EDP Sciences, 2018, p. 01077.
- [31] A. Dairi, F. Harrou, Y. Sun, S. Khadraoui, Short-term forecasting of photovoltaic solar power production using variational auto-encoder driven deep learning approach, *Applied Sciences* 10 (2020) 8400.
- [32] Y. Chen, X. Wang, B. Zhang, An unsupervised deep learning approach for scenario forecasts, in: 2018 Power Systems Computation Conference (PSCC), IEEE, 2018, pp. 1–7.
- [33] C. Jiang, Y. Mao, Y. Chai, M. Yu, Day-ahead renewable scenario forecasts based on generative adversarial networks, *International Journal of Energy Research* 45 (2021) 7572–7587.
- [34] J. Á. G. Ordiano, L. Gröll, R. Mikut, V. Hagenmeyer, Probabilistic energy forecasting using the nearest neighbors quantile filter and quantile regression, *International Journal of Forecasting* 36 (2020) 310–323.
- [35] Y. Zhang, Q. Ai, F. Xiao, R. Hao, T. Lu, Typical wind power scenario generation for multiple wind farms using conditional improved wasserstein generative adversarial network, *International Journal of Electrical Power & Energy Systems* 114 (2020) 105388.
- [36] Y. Wang, G. Hug, Z. Liu, N. Zhang, Modeling load forecast uncertainty using generative adversarial networks, *Electric Power Systems Research* 189 (2020) 106732.
- [37] Y. Qi, W. Hu, Y. Dong, Y. Fan, L. Dong, M. Xiao, Optimal configuration of concentrating solar power in multienergy power systems with an improved variational autoencoder, *Applied Energy* 274 (2020) 115124.
- [38] I. Goodfellow, Y. Bengio, A. Courville, *Deep learning*, volume 1, MIT press Cambridge, 2016.
- [39] A. Zhang, Z. C. Lipton, M. Li, A. J. Smola, *Dive into Deep Learning*, 2020. <https://d2l.ai>.
- [40] D. P. Kingma, T. Salimans, R. Jozefowicz, X. Chen, I. Sutskever, M. Welling, Improving variational inference with inverse autoregressive flow, *arXiv preprint arXiv:1606.04934* (2016).
- [41] A. Wehenkel, G. Louppe, Unconstrained monotonic neural networks, in: *Advances in Neural Information Processing Systems*, 2019, pp. 1545–1555.
- [42] G. Papamakarios, T. Pavlakou, I. Murray, Masked autoregressive flow for density estimation, in: *Advances in Neural Information Processing Systems*, 2017, pp. 2338–2347.
- [43] F. Pérez-Cruz, Kullback-leibler divergence estimation of continuous distributions, in: 2008 IEEE international symposium on information theory, IEEE, 2008, pp. 1666–1670.
- [44] I. Gulrajani, F. Ahmed, M. Arjovsky, V. Dumoulin, A. Courville, Improved training of wasserstein gans, *arXiv preprint arXiv:1704.00028* (2017).
- [45] T. Gneiting, A. E. Raftery, Strictly proper scoring rules, prediction, and estimation, *Journal of the American statistical Association* 102 (2007) 359–378.
- [46] P. Lauret, M. David, P. Pinson, Verification of solar irradiance probabilistic forecasts, *Solar Energy* 194 (2019) 254–271.
- [47] P. Geurts, D. Ernst, L. Wehenkel, Extremely randomized trees, *Machine learning* 63 (2006) 3–42.
- [48] F. X. Diebold, R. S. Mariano, Comparing predictive accuracy,

- Journal of Business & economic statistics 20 (2002) 134–144.
- [49] F. Ziel, R. Weron, Day-ahead electricity price forecasting with high-dimensional structures: Univariate vs. multivariate modeling frameworks, *Energy Economics* 70 (2018) 396–420.
- [50] M. Landry, T. P. Erlinger, D. Patschke, C. Varrichio, Probabilistic gradient boosting machines for gefcom2014 wind forecasting, *International Journal of Forecasting* 32 (2016) 1061–1066.
- [51] A. Wehenkel, G. Louppe, Graphical normalizing flows, *arXiv preprint arXiv:2006.02548* (2020).
- [52] L. Buitinck, G. Louppe, M. Blondel, F. Pedregosa, A. Mueller, O. Grisel, V. Niculae, P. Prettenhofer, A. Gramfort, J. Grobler, R. Layton, J. VanderPlas, A. Joly, B. Holt, G. Varoquaux, API design for machine learning software: experiences from the scikit-learn project, in: *ECML PKDD Workshop: Languages for Data Mining and Machine Learning*, 2013, pp. 108–122.
- [53] A. Paszke, S. Gross, F. Massa, A. Lerer, J. Bradbury, G. Chanan, T. Killeen, Z. Lin, N. Gimelshein, L. Antiga, A. Desmaison, A. Kopf, E. Yang, Z. DeVito, M. Raison, A. Tejani, S. Chilamkurthy, B. Steiner, L. Fang, J. Bai, S. Chintala, Pytorch: An imperative style, high-performance deep learning library, in: *Advances in Neural Information Processing Systems 32*, Curran Associates, Inc., 2019, pp. 8024–8035.
- [54] G. Papamakarios, E. Nalisnick, D. J. Rezende, S. Mohamed, B. Lakshminarayanan, Normalizing flows for probabilistic modeling and inference, *arXiv preprint arXiv:1912.02762* (2019).
- [55] I. Kobyzev, S. Prince, M. Brubaker, Normalizing flows: An introduction and review of current methods, *IEEE Transactions on Pattern Analysis and Machine Intelligence* (2020).
- [56] M. Arjovsky, L. Bottou, Towards principled methods for training generative adversarial networks, *arXiv preprint arXiv:1701.04862* (2017).
- [57] M. Arjovsky, S. Chintala, L. Bottou, Wasserstein generative adversarial networks, in: *International conference on machine learning*, PMLR, 2017, pp. 214–223.
- [58] C. Villani, *Optimal transport: old and new*, volume 338, Springer Science & Business Media, 2008.
- [59] D. P. Kingma, J. Ba, Adam: A method for stochastic optimization, *arXiv preprint arXiv:1412.6980* (2014).
- [60] M. Zamo, P. Naveau, Estimation of the continuous ranked probability score with limited information and applications to ensemble weather forecasts, *Mathematical Geosciences* 50 (2018) 209–234.

Appendix A. Background

Appendix A.1. NFs

NF computation

Evaluating the likelihood of a distribution modeled by a normalizing flow requires computing (2), *i.e.*, the normalizing direction, as well as its log-determinant. Increasing the number of sub-flows by K of the transformation results in only $O(K)$ growth in the computational complexity as the log-determinant of J_{f_θ} can be expressed as

$$\log |\det J_{f_\theta}(\mathbf{x})| = \log \left| \prod_{k=1}^K \det J_{f_{k,\theta}}(\mathbf{x}) \right|, \quad (\text{A.1a})$$

$$= \sum_{k=1}^K \log |\det J_{f_{k,\theta}}(\mathbf{x})|. \quad (\text{A.1b})$$

However, with no further assumption on f_θ , the computational complexity of the log-determinant is $O(K \cdot T^3)$, which can be intractable for large T . Therefore, the efficiency of these operations is particularly important during training where the likelihood is repeatedly computed. There are many possible implementations of NFs detailed by Papamakarios et al. [54], Kobyzev et al. [55] to address this issue.

Autoregressive flow

The Jacobian of the autoregressive transformation f_θ defined by (3) is lower triangular, and its log-absolute-determinant is

$$\log |\det J_{f_\theta}(\mathbf{x})| = \log \prod_{i=1}^T \left| \frac{\partial f^i}{\partial x_i}(x_i; h^i) \right|, \quad (\text{A.2a})$$

$$= \sum_{i=1}^T \log \left| \frac{\partial f^i}{\partial x_i}(x_i; h^i) \right|, \quad (\text{A.2b})$$

that is calculated in $O(T)$ instead of $O(T^3)$.

Affine autoregressive flow

A simple choice of transformer is the class of affine functions

$$f^i(x_i; h^i) = \alpha_i x_i + \beta_i, \quad (\text{A.3})$$

where $f^i(\cdot; h^i) : \mathbb{R} \rightarrow \mathbb{R}$ is parameterized by $h^i = \{\alpha_i, \beta_i\}$, α_i controls the scale, and β_i controls the location of the transformation. Invertibility is guaranteed if $\alpha_i \neq 0$, and this can be easily achieved by *e.g.* taking $\alpha_i = \exp(\tilde{\alpha}_i)$, where $\tilde{\alpha}_i$ is an unconstrained parameter

in which case $h^i = \{\tilde{\alpha}_i, \beta_i\}$. The derivative of the transformer with respect to x_i is equal to α_i . Hence the log-absolute-determinant of the Jacobian becomes

$$\log |\det J_{f_\theta}(\mathbf{x})| = \sum_{i=1}^T \log |\alpha_i| = \sum_{i=1}^T \tilde{\alpha}_i. \quad (\text{A.4})$$

Affine autoregressive flows are simple and computation efficient but are limited in expressiveness requiring many stacked flows to represent complex distributions. It is unknown whether affine autoregressive flows with multiple layers are universal approximators or not [54], in contrast to the UMNN autoregressive transformation implemented in this paper.

Appendix A.2. VAEs

Gradients computation

By using (6) $\mathcal{L}_{\theta,\varphi}$ is decomposed in two parts

$$\mathcal{L}_{\theta,\varphi}(\mathbf{x}, \mathbf{c}) = \mathbb{E}_{q_\varphi(\mathbf{z}|\mathbf{x}, \mathbf{c})} [\log p_\theta(\mathbf{x}|\mathbf{z}, \mathbf{c})] - \text{KL}[q_\varphi(\mathbf{z}|\mathbf{x}, \mathbf{c})||p(\mathbf{z})]. \quad (\text{A.5})$$

$\nabla_\theta \mathcal{L}_{\theta,\varphi}$ is estimated with the usual Monte Carlo gradient estimator. However, the estimation of $\nabla_\varphi \mathcal{L}_{\theta,\varphi}$ requires the reparameterization trick proposed by Kingma and Welling [10], where the random variable \mathbf{z} is re-expressed as a deterministic variable

$$\mathbf{z} = g_\varphi(\epsilon, \mathbf{x}), \quad (\text{A.6})$$

with ϵ an auxiliary variable with independent marginal p_ϵ , and $g_\varphi(\cdot)$ some vector-valued function parameterized by φ . Then, the first right hand side of (A.5) becomes

$$\mathbb{E}_{q_\varphi(\mathbf{z}|\mathbf{x}, \mathbf{c})} [\log p_\theta(\mathbf{x}|\mathbf{z}, \mathbf{c})] = \mathbb{E}_{p(\epsilon)} [\log p_\theta(\mathbf{x}|g_\varphi(\epsilon, \mathbf{x}), \mathbf{c})]. \quad (\text{A.7})$$

$\nabla_\varphi \mathcal{L}_{\theta,\varphi}$ is now estimated with Monte Carlo integration.

Conditional VAE implemented

Following Kingma and Welling [10], we implemented Gaussian multi-layered perceptrons (MLPs) for both the encoder NN_φ and decoder NN_θ . In this case, $p(\mathbf{z})$ is a centered isotropic multivariate Gaussian, $p_\theta(\mathbf{x}|\mathbf{z}, \mathbf{c})$ and $q_\varphi(\mathbf{x}|\mathbf{z}, \mathbf{c})$ are both multivariate Gaussian with a diagonal covariance and parameters $\boldsymbol{\mu}_\theta, \boldsymbol{\sigma}_\theta$ and $\boldsymbol{\mu}_\varphi, \boldsymbol{\sigma}_\varphi$, respectively. Note that there is no restriction on the encoder and decoder architectures, and they could as well be arbitrarily complex convolutional networks. Under these

assumptions, the conditional VAE implemented is

$$p(\mathbf{z}) = \mathcal{N}(\mathbf{z}; \mathbf{0}, \mathbf{I}), \quad (\text{A.8a})$$

$$p_\theta(\mathbf{x}|\mathbf{z}, \mathbf{c}) = \mathcal{N}(\mathbf{x}; \boldsymbol{\mu}_\theta, \boldsymbol{\sigma}_\theta^2 \mathbf{I}), \quad (\text{A.8b})$$

$$q_\varphi(\mathbf{z}|\mathbf{x}, \mathbf{c}) = \mathcal{N}(\mathbf{z}; \boldsymbol{\mu}_\varphi, \boldsymbol{\sigma}_\varphi^2 \mathbf{I}), \quad (\text{A.8c})$$

$$\boldsymbol{\mu}_\theta, \log \boldsymbol{\sigma}_\theta^2 = \text{NN}_\theta(\mathbf{x}, \mathbf{c}), \quad (\text{A.8d})$$

$$\boldsymbol{\mu}_\varphi, \log \boldsymbol{\sigma}_\varphi^2 = \text{NN}_\varphi(\mathbf{z}, \mathbf{c}). \quad (\text{A.8e})$$

Then, by using the valid reparameterization trick proposed by Kingma and Welling [10]

$$\epsilon \sim \mathcal{N}(\mathbf{0}, \mathbf{I}), \quad (\text{A.9a})$$

$$\mathbf{z} := \boldsymbol{\mu}_\varphi + \boldsymbol{\sigma}_\varphi \epsilon, \quad (\text{A.9b})$$

$\mathcal{L}_{\theta,\varphi}$ is computed and differentiated without estimation using the expressions

$$\text{KL}[q_\varphi(\mathbf{z}|\mathbf{x}, \mathbf{c})||p(\mathbf{z})] = -\frac{1}{2} \sum_{j=1}^d (1 + \log \boldsymbol{\sigma}_{\varphi,j}^2 - \boldsymbol{\mu}_{\varphi,j}^2 - \boldsymbol{\sigma}_{\varphi,j}^2), \quad (\text{A.10a})$$

$$\mathbb{E}_{p(\epsilon)} [\log p_\theta(\mathbf{x}|\mathbf{z}, \mathbf{c})] \approx -\frac{1}{2} \left\| \frac{\mathbf{x} - \boldsymbol{\mu}_\theta}{\boldsymbol{\sigma}_\theta} \right\|^2, \quad (\text{A.10b})$$

with d the dimensionality of \mathbf{z} .

Appendix A.3. GANs

GAN

The original GAN value function $V(\phi, \theta)$ proposed by Goodfellow et al. [11] is

$$V(\phi, \theta) = \underbrace{\mathbb{E}_{\mathbf{x}} [\log d_\phi(\mathbf{x}|\mathbf{c})] + \mathbb{E}_{\hat{\mathbf{x}}} [\log(1 - d_\phi(\hat{\mathbf{x}}|\mathbf{c}))]}_{:= -L_d}, \quad (\text{A.11a})$$

$$L_g := -\mathbb{E}_{\hat{\mathbf{x}}} [\log(1 - d_\phi(\hat{\mathbf{x}}|\mathbf{c}))], \quad (\text{A.11b})$$

where L_d is the cross-entropy, and L_g the probability the discriminator wrongly classifies the samples.

WGAN

The divergences which GANs typically minimize are responsible for their training instabilities for reasons investigated theoretically by Arjovsky and Bottou [56]. Arjovsky et al. [57] proposed instead using the *Earth mover* distance, also known as the Wasserstein-1 distance

$$W_1(p, q) = \inf_{\gamma \in \Pi(p, q)} \mathbb{E}_{(x,y) \sim \gamma} [|x - y|], \quad (\text{A.12})$$

where $\Pi(p, q)$ denotes the set of all joint distributions $\gamma(x, y)$ whose marginals are respectively p and q , $\gamma(x, y)$

indicates how much mass must be transported from x to y in order to transform the distribution p into q , $\|\cdot\|$ is the L1 norm, and $\|x - y\|$ represents the cost of moving a unit of mass from x to y . However, the infimum in (A.12) is intractable. Therefore, Arjovsky et al. [57] used the Kantorovich-Rubinstein duality [58] to propose the Wasserstein GAN (WGAN) by solving the min-max problem

$$\theta^* = \arg \min_{\theta} \max_{\phi \in \mathcal{W}} \mathbb{E}_{\mathbf{x}}[d_{\phi}(\mathbf{x}|\mathbf{c})] - \mathbb{E}_{\hat{\mathbf{x}}} [d_{\phi}(\hat{\mathbf{x}}|\mathbf{c})], \quad (\text{A.13})$$

where $\mathcal{W} = \{\phi : \|d_{\phi}(\cdot)\|_L \leq 1\}$ is the 1-Lipschitz space, and the classifier $d_{\phi}(\cdot) : \mathbb{R}^T \times \mathbb{R}^{|\mathbf{c}|} \rightarrow [0, 1]$ is replaced by a critic function $d_{\phi}(\cdot) : \mathbb{R}^T \times \mathbb{R}^{|\mathbf{c}|} \rightarrow \mathbb{R}$. However, the weight clipping used to enforce d_{ϕ} 1-Lipschitzness can lead sometimes the WGAN to generate only poor samples or failure to converge [44]. Therefore, we implemented the WGAN-GP to tackle this issue.

Appendix A.4. Hyper-parameters

Table A.4 provides the hyper-parameters of the NF, VAE, and GAN implemented. The Adam optimizer [59] is used to train the generative models with a batch size of 10 % of the learning set. The NF implemented

	Wind	PV	Load
Embedding Net	4×300	4×300	4×300
Embedding size	40	40	40
(a) Integrand Net	3×40	3×40	3×40
Weight decay	5.10^{-4}	5.10^{-4}	5.10^{-4}
Learning rate	10^{-4}	5.10^{-4}	10^{-4}
Latent dimension	20	40	5
(b) E/D Net	1×200	2×200	1×500
Weight decay	$10^{-3.4}$	$10^{-3.5}$	10^{-4}
Learning rate	$10^{-3.4}$	$10^{-3.3}$	$10^{-3.9}$
Latent dimension	64	64	256
(c) G/D Net	2×256	3×256	2×1024
Weight decay	10^{-4}	10^{-4}	10^{-4}
Learning rate	2.10^{-4}	2.10^{-4}	2.10^{-4}

Table A.4: (a) NF, (b) VAE, and (c) GAN hyper-parameters.

is a one-step monotonic normalizer using the UMN-NMAF³. The embedding size $|h^i|$ is set to 40, and the

³<https://github.com/AWehenkel/Normalizing-Flows>

embedding neural network is composed of l layers of n neurons ($l \times n$). The same integrand neural network $\tau^i(\cdot) \forall i = 1, \dots, T$ is used and composed of 3 layers of $|h^i|$ neurons (3×40). Both the encoder and decoder of the VAE are feed-forward neural networks ($l \times n$), ReLU activation functions for the hidden layers, and no activation function for the output layer. Both the generator and discriminator of the GAN are feed-forward neural networks ($l \times n$). The activation functions of the hidden layers of the generator (discriminator) are ReLU (Leaky ReLU). The activation function of the discriminator output layer is ReLU, and there is no activation function for the generator output layer. The generator is trained once after the discriminator is trained five times to stabilize the training process, and the gradient penalty coefficient λ in (7) is set to 10 as suggested by [44].

Appendix B. Quality and value assessment

Appendix B.1. Quality metrics

Continuous rank probability score

Gneiting and Raftery [45] proposed a formulation called the energy form of the CRPS (NRG) since it is just the one-dimensional case of the energy score

$$\text{CRPS}^{\text{NRG}}(\hat{F}_X, \mathbf{x}) = \mathbb{E}_X[|Z - \mathbf{x}|] - \frac{1}{2} \mathbb{E}_X[|Z - Z'|], \quad (\text{B.1})$$

where \hat{F}_X is the empirical cumulative distribution function of the random variable X , Z and Z' are two independent copies of a random variable with distribution function \hat{F} and finite first moment, and \mathbb{E}_X is the expectation according to the probabilistic distribution of the random variable X . Let $\{\hat{\mathbf{x}}^i\}_{i=1}^M$ be the set of M scenarios generated for a given day of the testing set. The estimator of (B.1) provided by Zamo and Naveau [60] is implemented

$$\begin{aligned} \text{CRPS}^{\text{eNRG}}(\{\hat{\mathbf{x}}^i\}_{i=1}^M, \mathbf{x}) &= \frac{1}{M} \sum_{i=1}^M |\hat{\mathbf{x}}^i - \mathbf{x}| \\ &\quad - \frac{1}{2M^2} \sum_{i,j=1}^M |\hat{\mathbf{x}}^i - \hat{\mathbf{x}}^j|. \end{aligned} \quad (\text{B.2})$$

Quantile score

Based on the generated scenarios for a given day of the testing set, 99 quantiles (1, 2, ..., 99th quantile) are computed $\{\hat{\mathbf{x}}^q\}_{q=1}^{99}$ with q the quantile index ($q = 0.01, \dots, 0.99$), and the quantile score is defined by

$$\rho_q(\hat{\mathbf{x}}^q, \mathbf{x}) = \begin{cases} (1 - q) \times (\hat{\mathbf{x}}^q - \mathbf{x}) & \mathbf{x} < \hat{\mathbf{x}}^q \\ q \times (\mathbf{x} - \hat{\mathbf{x}}^q) & \mathbf{x} \geq \hat{\mathbf{x}}^q \end{cases}. \quad (\text{B.3})$$

Classifier-based metric

A conditional classifier, taking into account the weather forecasts, per generative model is trained with a ratio of true and generated samples set to one. To take into account the variability from one scenario to another for a given context, 50 different pairs of learning and testing sets are built with 50 generated scenarios per day $\left\{ \{\hat{\mathbf{x}}_d^i\}_{d \in \text{LS}}, \{\hat{\mathbf{x}}_d^i\}_{d \in \text{TS}} \right\}_{i=1}^{50}$. For each pair i and model g , a classifier d_g^i is trained and outputs ROC_g^i and AUC_g^i . The Extra-Trees classifier is made of 1000 unconstrained trees with the hyper-parameters "max_depth" set to "None", and "n_estimators" to 1000.

Multivariate Diebold-Mariano test

For a given day d , let $\epsilon_d^g = [\epsilon_{d,1}^g, \dots, \epsilon_{d,24}^g]^\top$, $\epsilon_d^h = [\epsilon_{d,1}^h, \dots, \epsilon_{d,24}^h]^\top$ be the vectors of errors for a metric, such as the CRPS or QS, of models g and h , respectively. Then the multivariate loss differential series

$$\Delta(g, h)_d = \|\epsilon_d^g\|_1 - \|\epsilon_d^h\|_1, \quad (\text{B.4})$$

defines the differences of errors using the $\|\cdot\|_1$ norm. Then, for each model pair, the p -value of two-sided DM tests is computed by assuming, as in the standard DM test, that the loss differential series is covariance stationary.

Appendix B.2. Retailer formulation

Sets and indices

Name	Description
t	Time period index.
ω	Scenario index.
T	Number of time periods per day.
$\#\Omega$	Number of scenarios.
\mathcal{T}	Set of time periods, $\mathcal{T} = \{1, 2, \dots, T\}$.
Ω	Set of scenarios, $\Omega = \{1, 2, \dots, \#\Omega\}$.

Parameters

Name	Description
e_t^{\min}, e_t^{\max}	Minimum/maximum day-ahead bid [MWh].
y_t^{\min}, y_t^{\max}	Minimum/maximum retailer net position [MWh].
$y_{\max}^{\text{dis}}, y_{\max}^{\text{cha}}$	BESS maximum (dis)charging power [MW].
$\eta^{\text{dis}}, \eta^{\text{cha}}$	BESS (dis)charging efficiency [-].
s^{\min}, s^{\max}	BESS minimum/maximum capacity [MWh].

$s^{\text{ini}}, s^{\text{end}}$	BESS initial/final state of charge [MWh].
π_t	Day-ahead price [€/MWh].
$\bar{q}_t, \bar{\lambda}_t$	Negative/positive imbalance price [€/MWh].
Δt	Duration of a time period [hour].

Variables

For the sake of clarity the subscript ω is omitted.

Name	Range	Description
e_t	$[e_t^{\min}, e_t^{\max}]$	Day-ahead bid [MWh].
y_t	$[y_t^{\min}, y_t^{\max}]$	Retailer net position [MWh].
y_t^{PV}	$[0, 1]$	PV generation [MW].
y_t^{w}	$[0, 1]$	Wind generation [MW].
y_t^{cha}	$[0, y_{\max}^{\text{cha}}]$	Charging power [MW].
y_t^{dis}	$[0, y_{\max}^{\text{dis}}]$	Discharging power [MW].
s_t	$[s^{\min}, s^{\max}]$	BESS state of charge [MWh].
d_t^-, d_t^+	\mathbb{R}_+	Short/long deviation [MWh].
y_t^b	$\{0, 1\}$	BESS binary variable [-].

Problem formulation

The mixed-integer linear programming (MILP) optimization problem to solve is

$$\max_{e_t \in \mathcal{X}, y_{t,\omega} \in \mathcal{Y}(e_t)} \sum_{\omega \in \Omega} \alpha_\omega \sum_{t \in \mathcal{T}} \left[\pi_t e_t - \bar{q}_t d_{t,\omega}^- - \bar{\lambda}_t d_{t,\omega}^+ \right], \quad (\text{B.5a})$$

$$\mathcal{X} = \left\{ e_t : e_t \in [e_t^{\min}, e_t^{\max}] \right\}, \quad (\text{B.5b})$$

$$\mathcal{Y}(e_t) = \left\{ y_{t,\omega} : (\text{B.6a}) - (\text{B.6m}) \right\}. \quad (\text{B.5c})$$

The optimization variables are e_t , day-ahead bid of the net position, $\forall \omega \in \Omega$, $y_{t,\omega}$, retailer net position in scenario ω , $d_{t,\omega}^-$, short deviation, $d_{t,\omega}^+$, long deviation, $y_{t,\omega}^{\text{PV}}$, PV generation, $y_{t,\omega}^{\text{w}}$, wind generation, $y_{t,\omega}^{\text{cha}}$, battery energy storage system (BESS) charging power, $y_{t,\omega}^{\text{dis}}$, BESS discharging power, $s_{t,\omega}$, BESS state of charge, and $y_{t,\omega}^b$ a binary variable to prevent from charging and discharging simultaneously. The imbalance penalty is modeled by the constraints (B.6a)-(B.6b) $\forall \omega \in \Omega$, that define the short and long deviations variables $d_{t,\omega}^-, d_{t,\omega}^+ \in \mathbb{R}_+$. The energy balance is provided by (B.6c) $\forall \omega \in \Omega$. The set of constraints that bound $y_{t,\omega}^{\text{PV}}$ and $y_{t,\omega}^{\text{w}}$ variables are (B.6d)-(B.6e) $\forall \omega \in \Omega$ where $\hat{y}_{t,\omega}^{\text{PV}}$ and $\hat{y}_{t,\omega}^{\text{w}}$ are PV and wind generation scenarios. The load is assumed to be non-flexible and is a parameter (B.6f) $\forall \omega \in \Omega$ where $\hat{y}_{t,\omega}^l$ are load scenarios. The BESS constraints are provided by (B.6g)-(B.6j), and the BESS dynamics by (B.6k)-

(B.6m) $\forall \omega \in \Omega$.

$$-d_{t,\omega}^- \leq -(e_t - y_{t,\omega}), \forall t \in \mathcal{T} \quad (\text{B.6a})$$

$$-d_{t,\omega}^+ \leq -(y_{t,\omega} - e_t), \forall t \in \mathcal{T} \quad (\text{B.6b})$$

$$\begin{aligned} \frac{y_{t,\omega}}{\Delta t} &= y_{t,\omega}^{\text{pv}} + y_{t,\omega}^{\text{w}} - y_{t,\omega}^{\text{l}} \\ &\quad + y_{t,\omega}^{\text{dis}} - y_{t,\omega}^{\text{cha}}, \forall t \in \mathcal{T} \end{aligned} \quad (\text{B.6c})$$

$$y_{t,\omega}^{\text{pv}} \leq \hat{y}_{t,\omega}^{\text{pv}}, \forall t \in \mathcal{T} \quad (\text{B.6d})$$

$$y_{t,\omega}^{\text{w}} \leq \hat{y}_{t,\omega}^{\text{w}}, \forall t \in \mathcal{T} \quad (\text{B.6e})$$

$$y_{t,\omega}^{\text{l}} = \hat{y}_{t,\omega}^{\text{l}}, \forall t \in \mathcal{T} \quad (\text{B.6f})$$

$$y_{t,\omega}^{\text{cha}} \leq y_{t,\omega}^{\text{b}} y_{t,\omega}^{\text{cha}}, \forall t \in \mathcal{T} \quad (\text{B.6g})$$

$$y_{t,\omega}^{\text{dis}} \leq (1 - y_{t,\omega}^{\text{b}}) y_{t,\omega}^{\text{dis}}, \forall t \in \mathcal{T} \quad (\text{B.6h})$$

$$-s_{t,\omega} \leq -s^{\text{min}}, \forall t \in \mathcal{T} \quad (\text{B.6i})$$

$$s_{t,\omega} \leq s^{\text{max}}, \forall t \in \mathcal{T} \quad (\text{B.6j})$$

$$\frac{s_{1,\omega} - s^{\text{ini}}}{\Delta t} = \eta^{\text{cha}} y_{1,\omega}^{\text{cha}} - \frac{y_{1,\omega}^{\text{dis}}}{\eta^{\text{dis}}}, \quad (\text{B.6k})$$

$$\frac{s_{t,\omega} - s_{t-1,\omega}}{\Delta t} = \eta^{\text{cha}} y_{t,\omega}^{\text{cha}} - \frac{y_{t,\omega}^{\text{dis}}}{\eta^{\text{dis}}}, \forall t \in \mathcal{T} \setminus \{1\} \quad (\text{B.6l})$$

$$s_{T,\omega} = s^{\text{end}} = s^{\text{ini}}. \quad (\text{B.6m})$$

Notice that, if $\bar{\lambda}_t < 0$, the surplus quantity is remunerated with a non-negative price. In practice, such a scenario could be avoided provided that the energy retailer has curtailment capabilities, and $(\bar{q}_t, \bar{\lambda}_t)$ are strictly positive in our case study. The deterministic formulation with perfect forecasts, the oracle (O), is a specific case of the stochastic formulation by considering only one scenario where $y_{t,\omega}^{\text{pv}}$, $y_{t,\omega}^{\text{w}}$, and $y_{t,\omega}^{\text{l}}$ become the actual values of PV, wind, and load $\forall t \in \mathcal{T}$. The optimization variables are e_t , y_t , d_t^- , d_t^+ , y_t^{pv} , and y_t^{w} , y_t^{cha} , y_t^{dis} , s_t , and y_t^{b} .

Dispatching

Once the bids e_t have been computed by the planner, the dispatching consists of computing the second stage variables given observations of the PV, wind power, and load. The dispatch formulation is a specific case of the stochastic formulation with e_t as parameter and by considering only one scenario where $y_{t,\omega}^{\text{pv}}$, $y_{t,\omega}^{\text{w}}$, and $y_{t,\omega}^{\text{l}}$ become the actual values of PV, wind, and load $\forall t \in \mathcal{T}$. The optimization variables are y_t , d_t^- , d_t^+ , y_t^{pv} , and y_t^{w} , y_t^{cha} , y_t^{dis} , s_t , and y_t^{b} .

Appendix C. Quality results

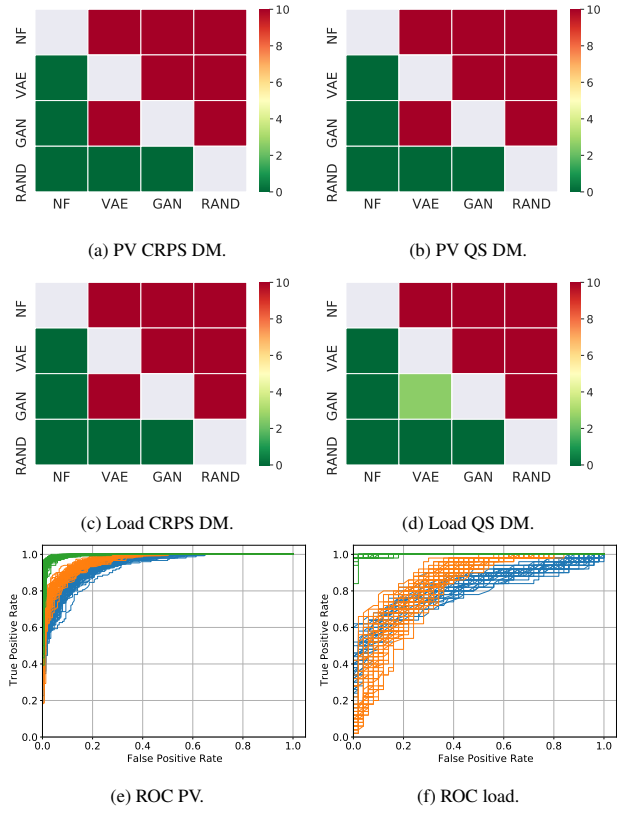


Figure C.8: PV and load tracks DM tests and classifier-based metric.

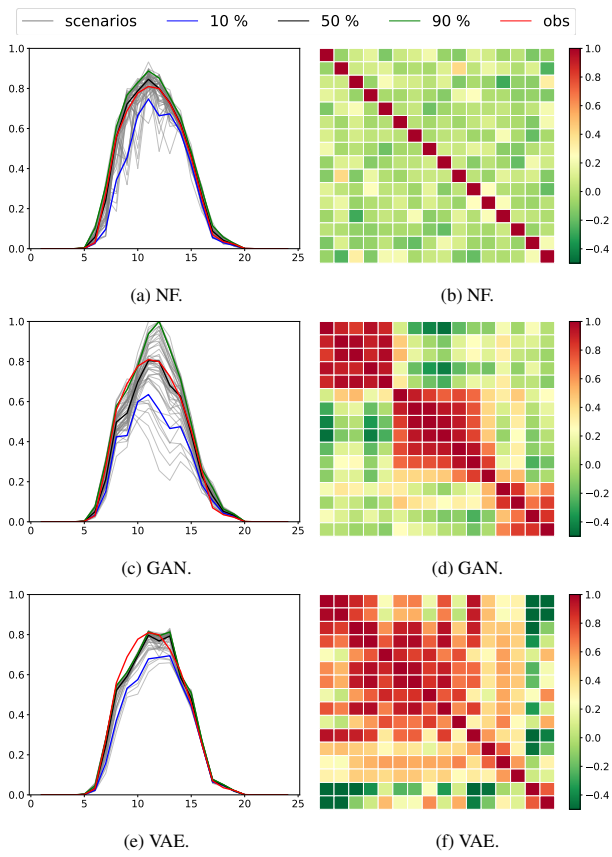


Figure C.9: PV scenarios and corresponding correlation matrices.

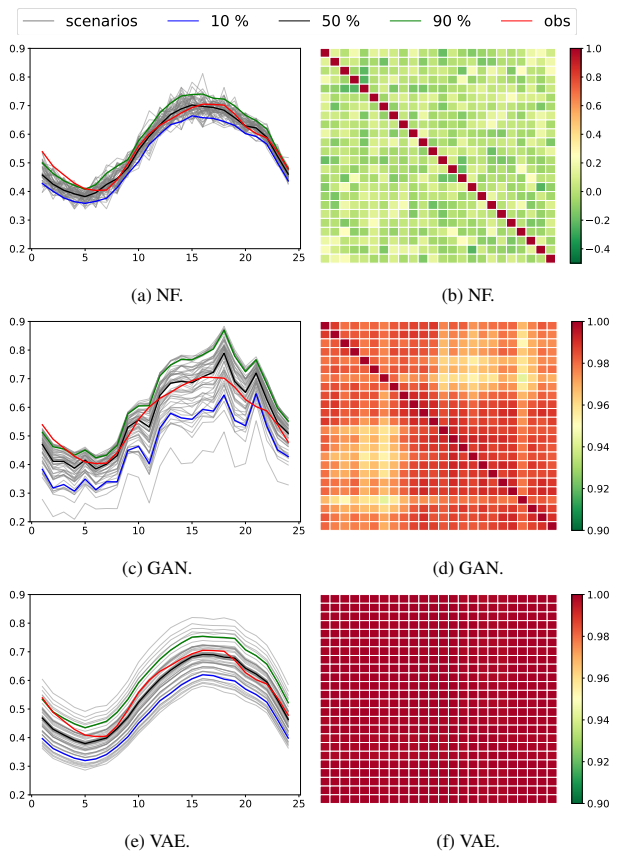


Figure C.10: Load scenarios and corresponding correlation matrices.